JOURNAL OF COLLOID AND INTERFACE SCIENCE **182,** 526–538 (1996)
ARTICLE NO. 0497

Experimental Confirmation of the Oscillating Bubble Technique with Comparison to the Pendant Bubble Method: The Adsorption Dynamics of 1-Decanol

DAVID O. JOHNSON AND KATHLEEN J. STEBE[1]

Johns Hopkins University, Baltimore, Maryland 21018

Received December 14, 1995; accepted March 28, 1996

A new oscillating bubble method is used to measure surfactant mass transfer kinetics at liquid–gas interfaces. A spherical bubble is formed, equilibrated, and oscillated radially with a small amplitude. The radial oscillations cause the gas-phase pressure to cycle about its equilibrium because of the periodic changes in bubble curvature and surface tension. The phase angle θ between the radial and the pressure oscillations and the amplitude ratio of these two quantities are measured as a function of forcing frequency ω' and concentration $C'_{(0)}$. These data are analyzed according to a linear analysis presented in part I of this research (*J. Colloid Interface Sci.* 168, 21, 1994) to find surfactant diffusivities and adsorption/desorption coefficients. The required input data are the equilibrium adsorption isotherm and the corresponding surface equation of state. For 1-decanol at the air–aqueous interface, equilibrium surface tension data are obtained by video-enhanced pendant bubble tensiometry and fitted to the generalized Frumkin model. The oscillating bubble method is then used to determine the mass transfer kinetics of 1-decanol. For $\omega' \leqslant 1$ rad/s, the mass transfer is diffusion-controlled. Diffusivities found from the oscillating bubble data are in agreement with those obtained from pendant bubble relaxation data. For elevated $C'_{(0)}$ and $\omega' \geqslant 1.0$ rad/s, the mass transfer is controlled by both diffusion and the kinetics of adsorption–desorption. A mixed diffusion–kinetic model applied to these data yields a value for the desorption kinetic constant of $\alpha = 2.7\ s^{-1}$. These results are consistent with the shift in controlling mechanism from pure diffusion control at dilute concentrations to mixed diffusion–kinetic control at elevated concentrations. © 1996 Academic Press, Inc.

Key Words: **surfactants; bubbles; pendant bubble method; oscillating bubble method; dynamic surface tension; Marangoni effects; adsorption kinetics; diffusion; 1-decanol.**

1. INTRODUCTION

The dynamic surface tension at fluid interfaces is determined by the rate that surfactant molecules diffuse and adsorb onto the interface. In a previous paper, a theory was presented which allows the measurement of surfactant diffusion and adsorption kinetics using the controlled oscillations of a spherical bubble at the end of a capillary (1). In this paper, experimental results for the oscillating bubble method for aqueous 1-decanol solutions are presented.

In the method, a spherical bubble is formed and equilibrated at the tip of a needle immersed in surfactant solution. The bubble is forced to oscillate with a frequency ω' by periodically injecting and withdrawing a small volume of gas. The periodic surface expansion causes the surface tension to cycle about its equilibrium value. However, the surface tension is out of phase with the radius because of hindered adsorption/desorption and diffusion. The radial oscillation also creates a flow field which perturbs the liquid-phase pressure. All of these contribute to oscillations in the gas-phase pressure, which is therefore out of phase with the radius.

Assuming that mass transfer to the interface is controlled by both diffusion and adsorption/desorption, and performing a linear analysis of the equations of mass transfer and fluid dynamics about an equilibrium, quiescent base state, the phase angle and the amplitude ratio between the gas-phase pressure and the bubble radius can be related to the physicochemical parameters in the surfactant system, i.e., the fluid viscosity μ' and density ρ', and the surfactant mass transfer kinetics (the adsorption and desorption kinetic constants, $\beta'_{(0)}$, and $\alpha'_{(0)}$, respectively, and the diffusivity D'). (Throughout this paper, all primed variables are dimensional, and all unprimed variables are dimensionless.) This analysis is presented in the first part of this study (1), which will be referred to as **I**.

In this article, experimental phase angle and amplitude ratio profiles are obtained as a function of forcing frequency ω'. With equilibrium data as input, theoretical profiles are obtained using the analysis in **I**. By minimizing the difference between the experimental and theoretical profiles, the mass transfer kinetics of 1-decanol are determined. For all

[1] To whom correspondence should be addressed at Dept. of Chemical Engineering, Johns Hopkins University, G.W.C. Whiting School of Engineering, Rm. 3400, North Charles St., Baltimore, MD 21218-2689.

0021-9797/96 $18.00

concentrations studied, a diffusion-controlled model gives good agreement between theory and experiment for $\omega' \leqslant 1$ rad/s. These results are compared to those obtained from pendant bubble relaxation experiments, which also exhibit diffusion control, in good agreement with the oscillating bubble. However, at the elevated bulk concentration (2.09×10^{-7} mol/cm^3) the kinetics of adsorption/desorption must be accounted for to explain the phase angle and amplitude ratio data for $\omega' \geqslant 1.0$. Excellent agreement between a mixed kinetic–diffusion-control model and the data is found for this concentration. This supports the concept of a shift in controlling mechanism from diffusion control to mixed diffusion/kinetic control with increasing bulk concentration (2, 3). The greater sensitivity of the oscillating bubble to this shift in mechanism results from the ability of this method to sample the faster time scales at which the sorption kinetics become important.

2. LITERATURE REVIEW

The oscillating bubble method used in this study relies on the forced oscillations of a pendant bubble. It differs from the previous oscillating pendant bubble methods which appear in both the biomedical and the interfacial phenomena literature (4–18). A general review of oscillating bubble methods is given in **I**. Therefore, only a brief discussion of previous studies of forced oscillations of *pendant* bubbles is given below.

In the method developed by Enhorning and co-workers (4–7) to study the dynamic surface tension of lung surfactant (LS) systems, a bubble is formed in an LS solution and instantaneously oscillated with large-amplitude oscillations (typically 30% of the bubble base radius). The bubble oscillations are caused by the motion of a rod immersed in the solution. The maximum and the minimum bubble radius are recorded. The pressure of the solution is continuously monitored, and the gas phase is maintained at atmospheric pressure. Using these data, the apparent surface tension is calculated using the equilibrium Young–Laplace equation. The transient behavior of the bubble and steady-state oscillations are recorded to infer information about the rate of LS adsorption, the enrichment of the interface in saturated lipids over many oscillation cycles by ''squeeze out,'' and the amplitude of surface tension oscillations realizable by the LS formulation. Hall *et al.* (7) have discussed the roles of shape deformations and surface dilatational viscosities on the LS data obtained from this apparatus. Franses and his collaborators (8–10) have modeled the coupled nonlinear flow field created by the motion of the bubble interface and the surfactant mass transfer, and have studied both LS-related and other surfactant systems.

Lunkenheimer and co-workers (11–14) independently developed an experiment based on an oscillating pendant bubble. They infer surfactant mass transfer kinetics by measuring the difference in energy needed to oscillate two simultaneous hemispherical bubbles, one in pure water and one in surfactant solution, at a given amplitude. In their analysis, the additional energy expended by the surfactant system is related via an energy balance to the additional work required to expand the surfactant-laden interface. This additional work is related to the diffusion-limited dilatational elasticity of Lucassen and Hansen (18). From these elasticities, the mass transfer kinetics are inferred.

The oscillating bubble method presented here uses small-amplitude oscillations about a known equilibrium state. The experiment is amenable to precise quantitative interpretation in terms of the phase angle θ between the radius and the gas-phase pressure. The sole inputs are the equilibrium constants for the adsorption isotherm and surface equation of state. The required equilibrium surface tension data are obtained in this study by a pendant bubble apparatus.

3. APPARATUS

The apparatus for the oscillating bubble experiment is assembled on a vibration-damped optical table (TMC) (see Fig. 1). At the center of the apparatus is an optical-quality quartz cell (Rame-Hart Co.). The cell is filled with a surfactant solution in which a bubble is formed at the tip of an inverted needle. Two perpendicular light beams are arranged to illuminate the cell. The first beam, formed from a tungsten–halogen arc lamp of constant intensity (Newport 780), is collimated through a series of pinholes and lenses. It projects the bubble silhouette onto a video camera (CCD-71, Dage-MIT Inc.). The second collimated beam is produced by a tungsten lamp (Olympus) powered by a dc source. This beam projects the shadow of the bubble edge through an objective lens onto a photodiode (Oriel 71801 installed in a 71925 head).

The bubble is formed by a syringe pump (Sage Instruments 341A) connected via a solenoid valve (Lee Co. LFYA 16032H) to an inverted supporting needle (Rame-Hart Co.). Using an A/D–D/A board (Data Translation DT2801) to momentarily open the solenoid valve, a bubble is rapidly formed. A second valve (Altech) is configured in the line leading to the needle. This valve allows the gas phase to be connected to a custom-made cell which houses a piezoelectric piston (Burleigh PZL-030) and a piezoresistive pressure transducer (Endevco 8510B-1). The piston is driven sinusoidally at a frequency ω' by a function generator (Krone-Hite 2000). The piston, connected to the gas-phase line, causes the bubble radius to oscillate.

The pressure transducer and photodiode signals are recorded on the hard disk of a 386 PC via an A/D–D/A board. The voltage trace from the photodiode allows the phase of the radial oscillation to be determined without cum-

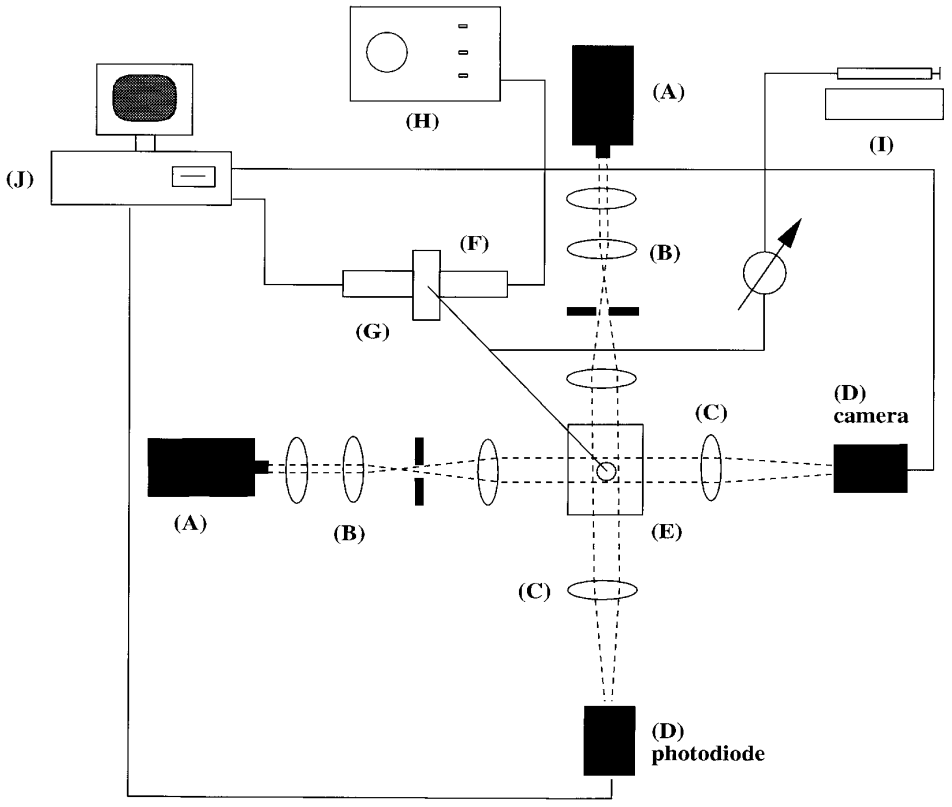

FIG. 1. The oscillating bubble apparatus is shown. There are two collimated light beams consisting of (A) a lamp, (B) collimating lenses, (C) an objective lens, and (D) a video camera (or, in the perpendicular direction, a photodiode). In the center is: (E) a quartz cell and inverted needle, (F) a piezoelectric piston, (G) a piezoresistive transducer, and (H) a function generator. The bubble formation apparatus is (I) a syringe pump and (J) a PC-interfaced solenoid valve. Data are acquired on a 386 PC clone.

bersome image analysis. The video camera, configured to a digitization board (Data Translation DT2861), allows images of the bubble shape to be recorded to disk.

4. MATERIALS AND METHODS

The alcohol 1-decanol (purity +99%), obtained from Aldrich Chemical Co., was used without modification. Purified water was obtained from a Milli-Q 50 (Millipore) that produces water with a resistivity of 18 MΩ · cm. The Teflon components and glassware were soaked overnight in a sulfuric acid–Nochromix solution and thoroughly rinsed in the purified water. All stainless steel pieces were repeatedly rinsed and sonicated in copious amounts of purified water. All solutions were made with purified water. The experiments were undertaken at atmospheric pressure at 22.0 ± 0.5°C.

The inverted needle was positioned in the solution-filled quartz cell at the intersection of the two light beams. A bubble with a radius in the range 0.7 to 1.0 mm was then formed. The bubble was oscillated at a set frequency with an amplitude of ~5% of its radius. In order to be certain that the bubble was oscillating about an equilibrium base state, the bubble was oscillated between 0.5 and 1 h. (The time scales chosen were always longer than those required for a pendant bubble to attain equilibrium according to pendant bubble relaxation experiments conducted in this laboratory.) Once the steady oscillations were established, the pressure transducer and photodiode signals were scanned over at least 0.5 h in order to verify that the oscillations were steady with time. The bubble image was recorded by strobing the video digitizer throughout the oscillation cycle. The video images were used to confirm the spherical shape of the bubble, to measure the base state radius, and to determine the amplitude of the radial oscillation. The frequency was then changed and the equilibration and scanning processes were repeated.

5. EQUILIBRIUM DATA: PENDANT BUBBLE

The equilibrium constants for the adsorption isotherm and the corresponding equation of state are required as input into the theoretical profiles. Equilibrium surface tension data were obtained using video-enhanced pendant bubble tensiometry (19, 20).

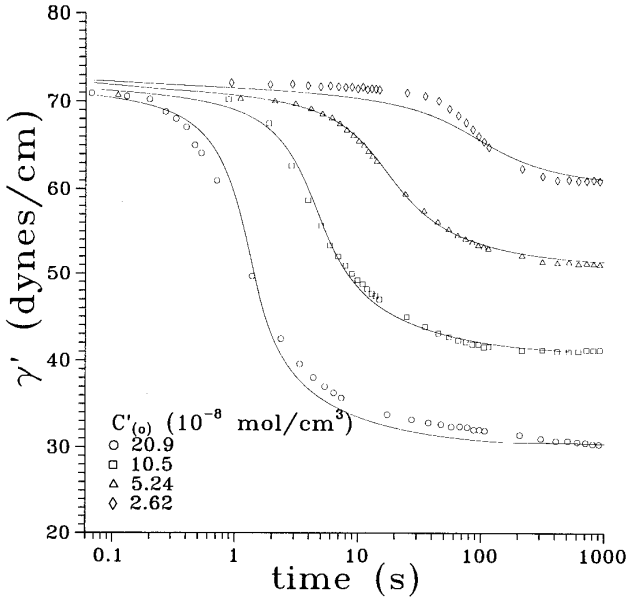

FIG. 2. Pendant bubble data for the surface tension relaxation profile over time are shown. The symbols represent the instantaneous surface tension. The curves represent the best diffusion control fit at each concentration in Fig. 2. The D' obtained from the data are reported in Table 3.

In this experiment, a bubble is rapidly formed at the tip of the inverted needle. The radius is large enough for buoyancy to appreciably distend the bubble shape. Image acquisition is always begun within 1 s of bubble formation, and is often initiated within $\frac{1}{15}$th of a second of bubble formation. When freshly formed, the bubble interface is surfactant-free. Over time, surfactant diffuses toward the bubble, adsorbs, and decreases the surface tension. The surface tension evolution causes the bubble to become increasingly elongated. From the bubble shape at each time step, the instantaneous surface tension can be determined.

Digital images of the bubble are recorded along with the time at which they were taken. The bubble edge is located, producing a coordinate map of the interface. This map is fitted to a numerical solution of the Young–Laplace equation for an axisymmetric body to obtain the surface tension corresponding to each image. In this manner, a surface tension versus time relaxation profile is constructed for each surfactant concentration studied (see Fig. 2). The equilibrium surface tensions, given by the long-time asymptotes, are presented in Fig. 3 as a function of bulk concentration $C'_{(0)}$.

Equilibrium Data and the Generalized Frumkin Model

The equilibrium data can be fitted to a theoretical adsorption isotherm and surface equation of state. Three frameworks have been shown to describe the equilibrium behavior of 1-decanol: the Frumkin, the generalized Frumkin, and the phase transition models. These models all capture the effects of cohesion between the long, saturated hydrocarbon chains. (For a thorough discussion of each of these models, see Lin *et al.* (21).) While the Frumkin and phase transition models describe the equilibrium data well, they do not agree well with the *dynamic* pendant bubble relaxation data obtained in our laboratory. All three models applied to the oscillating bubble data yield similar kinetic constants for surfactant mass transfer (see Johnson (22)). Only the results from the generalized Frumkin model are presented in this paper. The adsorption isotherm can be derived by equating the adsorption flux $P'(\Gamma'_{(0)}, C'_{(0)})$ and desorption flux $Q'(\Gamma'_{(0)}, C'_{(0)})$. The isotherm relates the surface concentration, $\Gamma'_{(0)}$, to the bulk concentration $C'_{(0)}$:

$$P'(\Gamma'_{(0)}, C'_{(0)}) = Q'(\Gamma'_{(0)}, C'_{(0)}). \qquad [1]$$

The adsorption rate is proportional to the amount of unoccupied surface, and is first order in bulk concentration immediately adjacent to the surface, C'_s. The desorption rate is first order in surface concentration. Therefore,

$$P' = \tilde{\beta}' \exp\left(-\frac{E'_a}{R'T'}\right) C'_s(\Gamma'_\infty - \Gamma')$$

$$Q' = \tilde{\alpha}' \exp\left(-\frac{E'_d}{R'T'}\right) \Gamma', \qquad [2]$$

where E'_a and E'_d are energies of activation of adsorption and desorption, respectively. The preexponential factors

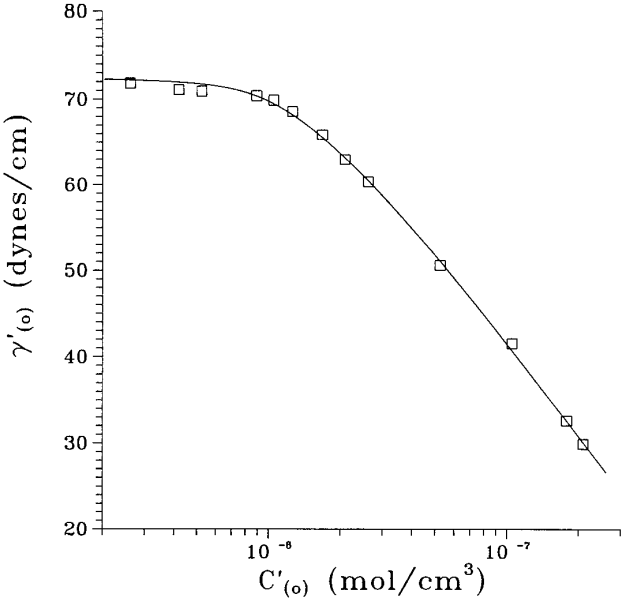

FIG. 3. The equilibrium surface tension data as a function of the bulk concentration of surfactant are shown. The symbols represent the data, and the curve represents the best fit of the generalized Frumkin isotherm to the data.

$\tilde{\beta}'$ and $\tilde{\alpha}'$ are the characteristic rates of adsorption and desorption. Here, Γ' is the surface concentration, Γ'_∞ is the surface concentration at maximum packing, R' is the gas constant, and T' is the temperature.

If the surfactant has nonideal interactions, the activation energies for adsorption and desorption depend on Γ'. Assuming that this dependence follows a power law, the energies can be written

$$E'_a = E^{0}_{a}{}' + \nu'_a \Gamma'^{n}$$
$$E'_d = E^{0}_{d}{}' + \nu'_d \Gamma'^{n}, \qquad [3]$$

where $E^{0}_{a}{}'$, $E^{0}_{d}{}'$, ν'_a, ν'_d, and n are constants. If Eq. [3] is substituted into Eq. [2] and the fluxes P' and Q' are equated, the generalized Frumkin isotherm results,

$$\frac{\Gamma'_{(0)}}{\Gamma'_\infty} = \frac{C'_{(0)}}{C'_{(0)} + a' \exp(K'[\Gamma'_{(0)}/\Gamma'_\infty]^n)}, \qquad [4]$$

where

$$K = (\nu'_a - \nu'_d)\Gamma_\infty/R'T',$$
$$a = \alpha'_{(0)}/\beta'_{(0)},$$
$$\alpha'_{(0)} = \tilde{\alpha}' \exp(E'^{0}_{d}/R'T'),$$
$$\beta'_{(0)} = \tilde{\beta}' \exp(E'^{0}_{a}/R'T').$$

The parameter K describes the presence of nonideal cohesive/repulsive intermolecular forces. For example, for interchain cohesion, the energy required to desorb increases more rapidly than that required to adsorb with Γ', resulting in $K < 0$.

Using the Gibbs–Duhem equation for the interface, the surface equation of state results,

$$\gamma'(t) = \gamma'_{\text{clean}} + \Gamma'_\infty R'T' \left[\ln\left(1 - \frac{\Gamma'}{\Gamma'_\infty}\right) - K' \frac{n}{n+1} (\Gamma'/\Gamma'_\infty)^{n+1} \right], \qquad [5]$$

where γ'_{clean} is the surface tension of the surfactant-free interface. Note that in this model, cohesion has three effects: it alters the kinetics of adsorption/desorption, the partitioning of surfactant, and the sensitivity of γ' to Γ'.

The equilibrium surface tension data are shown in Fig. 3 with the best fit generalized Frumkin equation of state. The isotherm constants are given in Table 1; they are in reasonable agreement with those of Lin *et al.* (21), whose isotherm constants are also reported in Table 1 for comparison.

TABLE 1
Generalized Frumkin Adsorption Isotherm Constants for 1-Decanol in Aqueous Solution

Isotherm	Generalized Frumkin (this study)	Generalized Frumkin (Lin *et al.* (19))
a' (mol/cm^3)	3.31×10^{-7}	4.092×10^{-7}
n	0.361	0.5
K	−4.19	−4.62
Γ'_∞ (mol/cm^2)	6.516×10^{-10}	7.05×10^{-10}

6. OSCILLATING BUBBLE DATA

The bubble is forced to oscillate with roughly 5% of its base radius. A digitized image of the bubble at its maximum and minimum radius is shown in the inset of Fig. 4. The amplitude ratio can be obtained from such digitized images of the bubble (providing the amplitude of the radial oscillation) and the pressure transducer output. The amplitude ratio data are discussed under Results and Discussion, below.

The phase angle θ between the radial and the pressure oscillations is calculated from the photodiode and the pressure transducer signals by fitting many wavelengths of each signal to a sine function,

$$V'_i = A'_i \sin(\omega' t' + \theta'_i) + M'_i, \qquad [6]$$

where i = PD or PT, and indicates the photodiode signal or pressure transducer signal, respectively. The voltage signal is denoted by V'_i, the amplitude is given by A'_i, and time is denoted t'. The voltage offset is denoted M'_i. The signal fitting results in a phase angle for each signal θ_{PD}, θ_{PT}, and the frequency ω' of each signal. The frequencies agree to within 0.1% with each other and with the input frequency of the function generator. The phase angle between the gas pressure and the radial oscillations θ is calculated simply by

$$\theta = \theta_{\text{PT}} - \theta_{\text{PD}}. \qquad [7]$$

Typical θ versus ω' graphs are presented in Fig. 4. In interpreting the phase angle graphs, recall that phase angles of 0 or π are equivalent ($\tan 0 = \tan \pi = 0$). A small phase lag therefore corresponds to phase angles that depart only slightly from 0 or π, and the largest phase lag is realized for $\theta = \pi/2$.

Consider the shape of the θ curve. At low ω', θ departs only slightly from π'; small lags are realized as mass transfer is rapid enough to keep the interface near equilibrium. At higher ω', the mass transfer time scales are comparable to

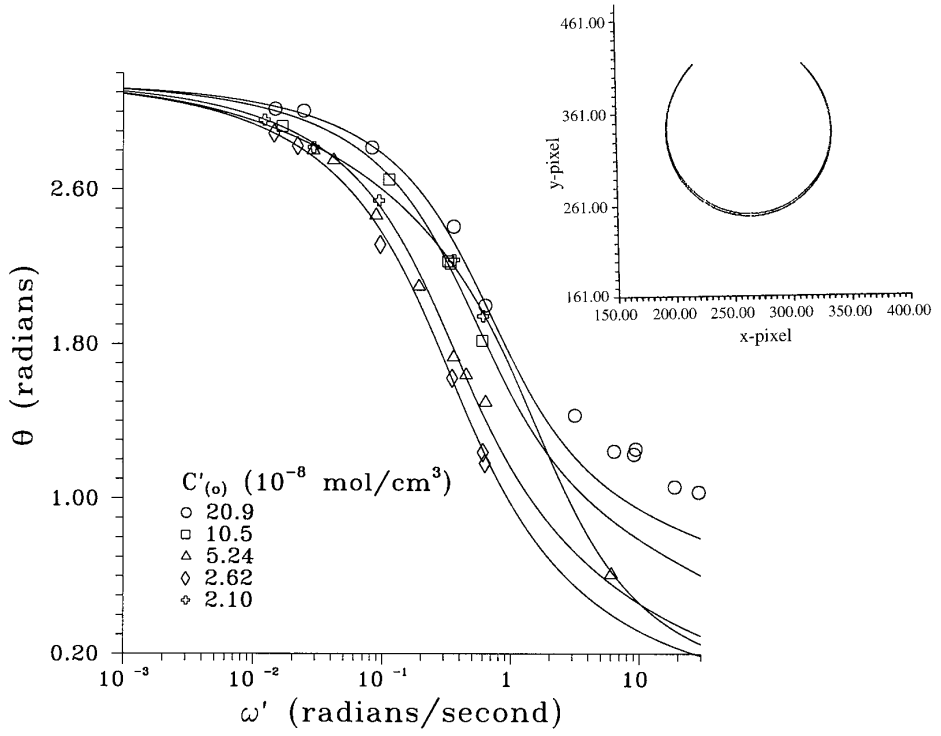

FIG. 4. A family of phase angle θ vs forcing frequency ω' curves at various bulk concentrations $C'_{(0)}$. The curves are the diffusion-control fits to the data. The D' are reported in Table 3. The inset is a digitized image of the oscillating bubble captured at its maximum and minimum radius.

$1/\omega'$; appreciable phase lags develop and θ approaches $\pi/2$. (Finally, at very high ω', orders of magnitude greater than those shown in Fig. 4, the inverse frequency exceeds the mass transfer time scales. The surface behaves as a insoluble monolayer and θ approaches zero or π. See **I**.).

7. COMPARISON OF THEORY AND EXPERIMENT

A. Oscillating Bubble

In order to determine the mass transfer coefficients for 1-decanol from the oscillating bubble data, the phase angle data must be compared to theoretical phase angle profiles. Equations for these profiles have been derived in **I** from a linear analysis of the governing mass transfer and Stokes equations about the equilibrium base state. Only the equations essential for generating these theoretical profiles are discussed here.

Generation of Theoretical θ versus ω' Curves

The tangent of θ is obtained by taking the ratio of the imaginary to the real parts of the gas-phase pressure perturbation caused by the oscillating bubble radius:

$$\tan\theta = -\frac{4\mathrm{Ca} + 4\mathrm{Ca}_s - 2E\Gamma_{(1)_{\mathrm{IM}}}}{\Pi + 2 + 2E\Gamma_{(1)_{\mathrm{RE}}}}. \qquad [8]$$

The dimensionless quantities

$$\Pi = \frac{\rho' A'^2_{(0)}}{\gamma'_{(0)}}\omega'^2, \quad \mathrm{Ca} = \frac{\mu' A'_{(0)}}{\gamma'_{(0)}}\omega',$$

$$\mathrm{Ca}_s = \frac{\kappa'_{(0)}}{\gamma'_{(0)}}\omega', \quad E = -\frac{\partial\gamma}{\partial\Gamma}\Big|_{(0)}\frac{\Gamma_{(0)}}{\gamma_{(0)}} \qquad [9]$$

are defined in terms of ρ', the density of the surfactant solution; $A'_{(0)}$, the base state radius of the bubble; $\gamma'_{(0)}$, the base state surface tension; μ', the solution viscosity; and $\kappa'_{(0)}$, the surface dilatational viscosity evaluated at the base state surface concentration.

The denominator of tan θ contains the elastic-like contributions to the gas-phase pressure perturbation, which include Π, the magnitude of the liquid-phase pressure perturbation at the interface; 2, the dimensionless Laplace pressure perturbation from the radial change; and $2E\Gamma_{(1)_{\mathrm{RE}}}$, the real part of the surface tension perturbation, expressed in terms of the perturbed surface concentration. In this expression, $\Gamma_{(1)_{\mathrm{RE}}}$ is the real part of the surface concentration perturbation caused by the hindered surfactant mass transfer to the interface, made dimensionless with its equilibrium surface concentration $\Gamma'_{(0)}$. The elasticity number, E, couples the surface tension to the surface concentration.

The numerator of tan θ contains the viscous-like contributions to the gas-phase pressure perturbation, including Ca, the capillary number, the ratio of the viscous stresses to the Laplace pressure; Ca_s, the surface capillary number, the corresponding ratio for the surface viscosity; and $2E\Gamma_{(1)_{IM}}$, the imaginary part of the surface tension perturbation, where $\Gamma_{(1)_{IM}}$ is the dimensionless imaginary part of the surface concentration perturbation.

The perturbations in the surface concentration can be related to the surfactant mass transfer kinetics through $\Gamma_{(1)_{IM}}$ and $\Gamma_{(1)_{RE}}$. Analytical expressions for these quantities can be obtained for diffusion-control or mixed diffusion–adsorption/desorption-control models, allowing θ to be obtained for the diffusivity D' and desorption coefficient $\alpha'_{(0)}$.

Simplification of the Phase Angle Expression for the Aqueous 1-Decanol System

(i) Ca_s can be neglected. The surface capillary number is defined in terms of the surface dilatational viscosity for a Newtonian interface, $\kappa'_{(0)}$. Surface viscosities would be expected to be most pronounced at elevated surface concentrations. Therefore, a model curve corresponding to oscillations about the equilibrium for the highest bulk concentration studied is generated for 1-decanol at air–aqueous interfaces. The surface viscosity is unknown, and various values for this parameter are input. The surface viscosity must become unrealistically large (greater than 10 surface poise) in order to cause a discernable change in the shape of the θ vs ω' curves for reasonable values of the surfactant diffusivity D' and adsorption–desorption parameters. (See Fig. 5, where the phase angle corresponding to $C_{(0)} = 2.09 \times 10^{-7}$ mol/cm^3 is graphed as a function of ω' and $\kappa'_{(0)}$). Therefore, $\kappa'_{(0)}$ can be neglected in the data analysis and Ca_s is equated to zero.

(ii) Ca can be neglected. By adopting the characteristic values for the physicochemical constants for 1-decanol solutions, the maximum magnitude of Ca realizable can be estimated. The solution viscosity is $\mu' = 0.01$ poise; the minimum value for the surface tension is approximately 25 dyn/cm; typical bubble radii are $R_0 = 0.1$ cm; and the maximum forcing frequencies considered are approximately $\omega' = 10$ rad s^{-1}. Using these values, the largest Ca encountered in this study is approximately 4×10^{-4}, a negligible contribution.

(iii) Π can be neglected. Performing a similar calculation for Π, and adopting a density of 1 g/cm^3, the largest contribution for Π is also 4×10^{-4}, a negligible factor.

The results reported in this paper were analyzed both including and excluding Ca and Π; neglecting these quantities has no impact on the results obtained.

Diffusion-Control Analysis of the Phase Angle Data

Assuming that the surfactant transport is diffusion-controlled, the sole unknown required to describe the phase angle θ is the diffusivity D'. For this case,

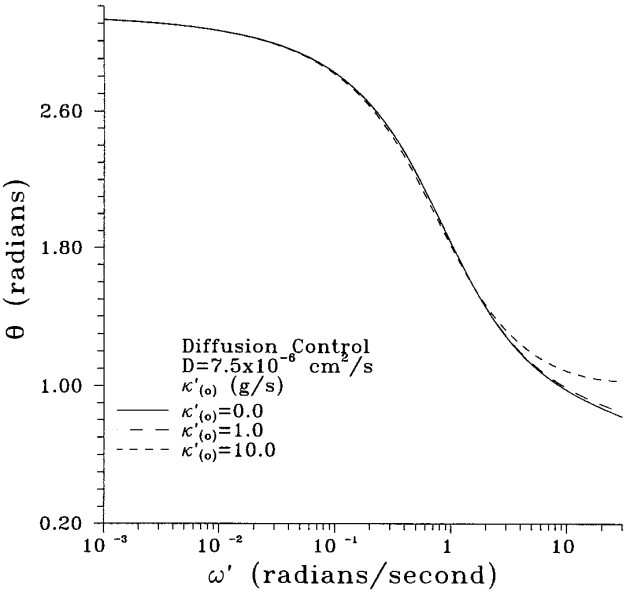

FIG. 5. Theoretical profiles of θ corresponding to $\kappa'_{(0)}$ of 0, 1, and 10 surface poise. All curves correspond to $C'_{(0)} = 2.09 \times 10^{-7}$ cm^2/s.

$$\Gamma_{(1)} = \Gamma_{(1)_{RE}} + i\Gamma_{(1)_{IM}}$$

$$\Gamma_{(1)_{RE}} = -\frac{2B(B-S)}{(B-S)^2 + (1+S)^2}$$

$$\Gamma_{(1)_{IM}} = \frac{2B(1+S)}{(B-S)^2 + (1+S)^2}, \qquad [10]$$

where

$$B = \frac{d_c \mathrm{Pe} h}{d_\Gamma}; \quad S = \sqrt{\frac{\mathrm{Pe}}{2}}$$

$$\mathrm{Pe} = \frac{\omega' A'^2_{(0)}}{D'}; \quad h = \frac{\Gamma'_{(0)}}{C'_{(0)} A'_{(0)}}. \qquad [11]$$

In these expressions Pe is the Peclet number and h is the dimensionless adsorption depth. The groups d_C and d_Γ are the characteristic sorptive fluxes which are obtained by perturbing $P'(\Gamma', C') - Q'(\Gamma', C')$ about the base state bulk and surface concentrations $\Gamma'_{(0)}$ and $C'_{(0)}$. The functional forms of d_C and d_Γ are given in Table 2. The elasticity number E defined in Eq. [9] is also reported in Table 2.

The diffusion control fit to the oscillating bubble data for $\omega' \leqslant 1$ rad/s (the data indicated by the symbols) is shown in Fig. 4. The best D' at each concentration is determined numerically by stepping through D' of order 10^{-6} cm^2/s, and locating the best D' to 10^{-7} cm^2/s. The agreement between theory and experiment is excellent. At each concentration, the diffusion coefficients are tabulated in Table 3.

TABLE 2
Expressions for d_C and d_Γ

Isotherm	Generalized Frumkin
d_C	$\dfrac{\alpha'}{\omega'}$
d_Γ	$-\dfrac{\alpha'}{\omega'}\left[1 + nK(\Gamma'_{(o)}/\Gamma'_\infty)^n + C'_{(o)}\dfrac{e^{-(K(\Gamma'_{(o)}/\Gamma'_\infty)^n)}}{a'}\right]$
E	$R'T'\left[\dfrac{1}{1-\Gamma'_{(o)}/\Gamma'_\infty} + nK(\Gamma'_{(o)}/\Gamma'_\infty)^n\right]\left(\dfrac{\Gamma'_{(o)}}{\gamma'_{(o)}}\right)$
Parameters	$a' = \dfrac{\alpha'_{(o)}}{\beta'_{(o)}},\ \alpha' = \alpha'_{(o)}\exp\left(-\dfrac{\nu'_d\Gamma'^n_{(o)}}{R'T'}\right),$
	$K = \dfrac{(\nu'_a - \nu'_d)\Gamma'^n_\infty}{R'T'}$

However, at faster forcing frequencies, the agreement between theory and experiment breaks down for the diffusion-controlled model. The phase angle is greater (i.e., closer to $\pi/2$) than that predicted by the diffusion-controlled curve, indicating that some other transport mechanism is contributing to θ. The predicted form of the curve for a surface dilatational viscosity is not consistent with the data (see Fig. 5). Therefore, a mixed kinetic–diffusion-control model is applied to the phase angle profile at $C'_{(0)} = 2.09 \times 10^{-7}$ mol/cm^3.

Mixed-Control Fit of the Phase Angle Data

For mixed-control mass transfer, the flux of surfactant to the bubble is determined both by bulk diffusion to the sublayer and by adsorption–desorption between the sublayer and the interface. The analysis is detailed in **I**; only the results are repeated here. The phase angle θ is given by Eq. [8]. The perturbations in the surface concentrations $\Gamma_{(1)_{RE}}$ and $\Gamma_{(1)_{IM}}$ are

$$\Gamma_{(1)} = \Gamma_{(1)_{RE}} + i\Gamma_{(1)_{IM}}$$

$$\Gamma_{(1)_{RE}} = -2\,\frac{[(1+S+L)^2 - Ld_\Gamma S + S^2]}{[(1+S+L) - d_\Gamma S]^2 + [S + d_\Gamma(1+S)]^2}$$

$$\Gamma_{(1)_{IM}} = \frac{[d_\Gamma S^2 + d_\Gamma(1+S)(1+S+L)]}{[(1+S+L) - d_\Gamma S]^2 + [S + d_\Gamma(1+S)]^2}, \qquad [12]$$

where $L = d_C\mathrm{Pe}h$ and $S = (\mathrm{Pe}/2)^{1/2}$, and the functional form of d_Γ and d_C are given in Table 2.

There are three unknowns which determine the mass transfer: D', $\alpha'_{(0)}$, and ν'_a or ν'_d. the difference of $\nu'_a - \nu'_d$ is proportional to K, which is known from the equilibrium study. However, the individual values of these parameters are required for dynamic analysis. In this analysis, as in MacLeod and Radke (23) and Lin *et al.* (24) it is assumed that cohesion primarily alters E'_d. Therefore, ν'_a is neglected and ν'_d is given by

$$K = -\frac{\nu'_d\Gamma'_\infty}{R'T'}, \quad \text{so}$$

$$\alpha' = \alpha'_0\exp\frac{K\Gamma'}{\Gamma'_\infty}. \qquad [13]$$

This reduces the unknowns to $\alpha'_{(0)}$ and D'. At $C'_{(0)} = 2.09 \times 10^{-7}$ mol/cm^3, a two-parameter fit of the data is performed by numerically stepping through D' of order 10^{-6} cm^2/s in steps of 10^{-7} cm^2/s and scanning the constant $\alpha'_{(0)}$ (which is independent of surface concentration) so that α' varies from 0.1 to 10 s^{-1} in steps of 0.1 s^{-1}. A diffusivity of 7.5×10^{-6} cm^2/s and a desorption kinetic constant of 2.7 s^{-1} were found to give the best fit. The mixed-control fit for the oscillating bubble data is graphed as the solid curve in Fig. 6. The graph of the error per point as a function of α' is given in Fig. 7b at the best diffusion coefficient. A clear minimum appears in the graph at the best value for α'.

A mixed-control analysis of the lower concentration data was also performed. This time, a single parameter fit, with D' fixed at 8.4×10^{-6} cm^2/s (the largest D' obtained for, diffusion-control fit) and stepping through the α' range as before. For these concentrations, no best fit value for α' is obtained. Rather, the error per point approaches some asymptote as α' increases. A typical error vs α' profile for these concentrations is reported in Figs. 7a and 7b. Thus, for the lower concentrations, the mixed-control model predicts a lower bound α'_b; any $\alpha' \geqslant \alpha'_b$ yields equally good agreement between theory and experiment. All of the lower bounds are less than the best fit value obtained from the highest concentration.

TABLE 3
Diffusivities for a Diffusion-Control Fit (D', 10^{-6} cm^2/s)

$C'_{(o)}$ ($\times 10^8$ mol/cm^3)	Oscillating bubble	Pendant bubble
2.10	7.5	—
2.62	6.4	6.6
5.24	7.8	7.7
10.5	8.4	6.7
20.9	6.5	5.8
D'_{ave}	7.3	6.7

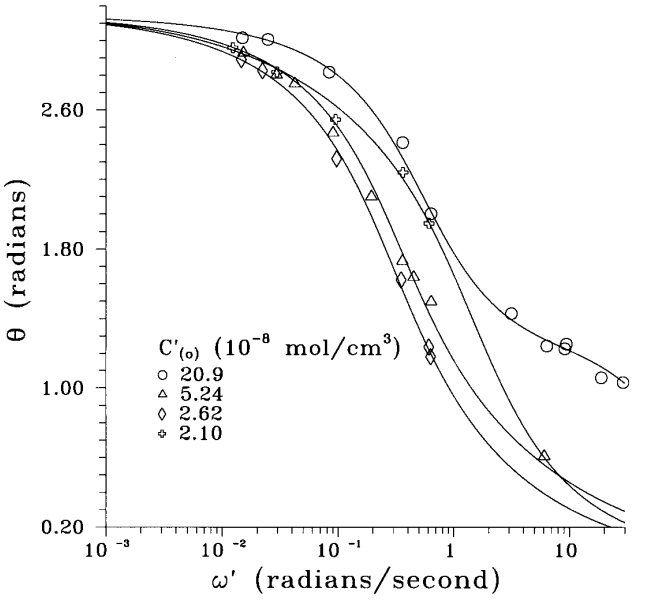

FIG. 6. The mixed-control fit of θ vs ω'. The symbols represent data; the curves are the theoretical profiles corresponding to the α' given in Table 4.

B. Pendant Bubble

Diffusion-Control Analysis of Pendant Bubble Relaxation Data

In this analysis, the bubble is treated as a sphere of radius R_s, the radius of a sphere with the same volume as the bubble. The interface is assumed to be initially surfactant-free:

$$\Gamma'(t' = 0) = 0. \quad [14]$$

The sublayer concentration is initially zero, and the bulk concentration C' is assumed to be uniform at $C'_{(0)}$:

$$C'_s(t' = 0) = C'|_{R'=R'_s}(t' = 0) = 0 \quad [15]$$

$$C'(r', t' = 0) = C'_0. \quad [16]$$

Far from the bubble, the bulk concentration remains uniform at $C'_{(0)}$:

$$\lim_{r\to\infty} C' = C'_{(0)}. \quad [17]$$

Surfactant adsorbs along the interface, partitioning according to the adsorption isotherm, Eq. [4].

Surfactant adsorption sets up a diffusive flux from the bulk toward the interface,

$$D' \frac{\partial C'}{\partial r'}\Big|_{R'=R'_s} = \frac{\partial \Gamma'}{\partial t'}, \quad [18]$$

where the bulk concentration is governed by Fick's law:

$$\frac{\partial C'}{\partial t'} = \frac{D'}{r'}\frac{\partial}{\partial r'}\left(r'\frac{\partial C'}{\partial r'}\right). \quad [19]$$

Equations [18] and [19] are solved simultaneously, subject to initial and boundary conditions, Eqs. [14]–[17], to

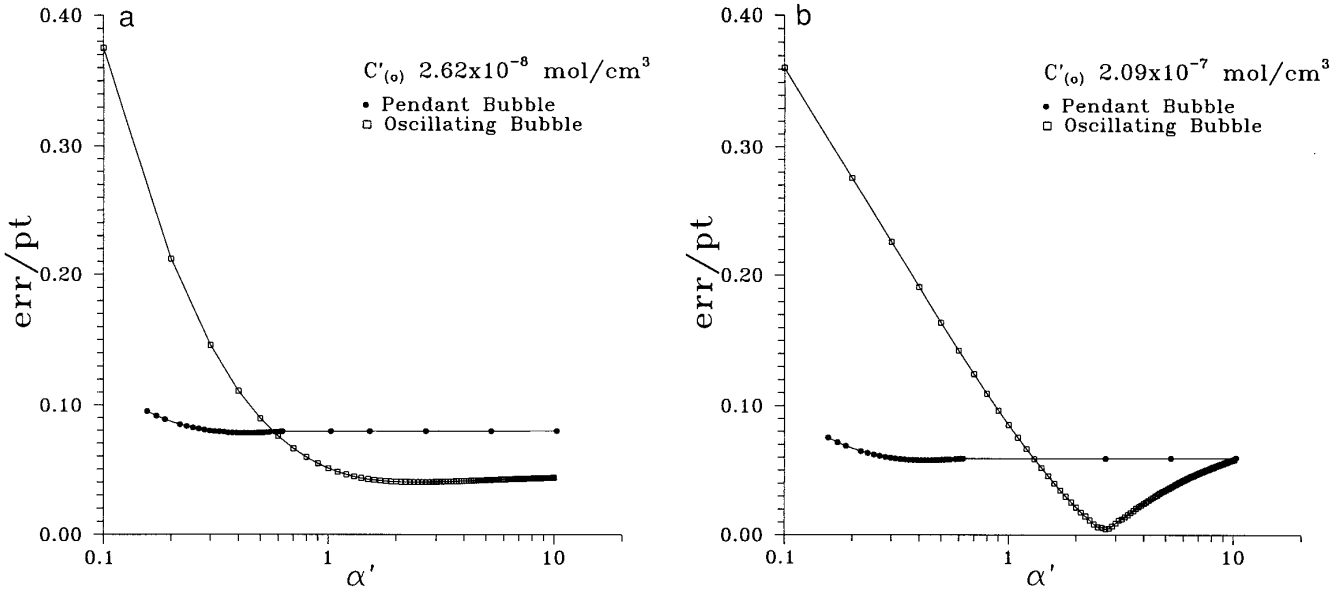

FIG. 7. The error per point as a function of the desorption kinetic constant α' for the mixed-control analysis of the oscillating bubble data and the pendant bubble relaxation profiles at (a) $C'_{(0)} = 2.62 \times 10^{-8}$ mol/cm^3 and (b) $C'_{(0)} = 2.09 \times 10^{-7}$ mol/cm^3.

find the evolution in $\Gamma'(t')$. The equation of state (Eq. [5]) is used to relate $\Gamma'(t')$ to $\gamma'(t')$.

This theoretical surface tension profile is then used to find the diffusion coefficient by numerically minimizing the error between the experimental and the numerical curves. An objective function equal to the squared normal distance between the experimental and the theoretical curves is numerically minimized with respect to D' by stepping through diffusion coefficients of O (10^{-6} cm^2/s) with steps of 10^{-7} cm^2/s.

The diffusion-control fit to the pendant bubble relaxation data is presented in Fig. 2; the diffusion coefficient for each concentration and each adsorption model is reported in Table 3.

Mixed-Control Analysis of the Pendant Bubble Data

In this mass transfer regime, the flux of surfactant to the interface must be amended to account for the finite adsorption–desorption rates. Therefore, Eq. [18] is replaced with

$$D' \frac{\partial C'}{\partial r'}\Big|_{R'=R'_s} = P'(\Gamma', C'_s) - Q'(\Gamma') = \frac{\partial \Gamma'}{\partial t'}, \quad [20]$$

where P' and Q' are given in Eqs. [2] and [3]. The initial sublayer concentration in this model is assumed to be the bulk concentration:

$$C'_s(t' = 0) = C'_{(0)}. \quad [21]$$

Equations [19] and [20] are integrated simultaneously over time subject to initial and boundary conditions, Eqs. [14], [16], [17], and [21].

In order to find values for the desorption kinetic constant, the diffusivity was set equal to 7.7×10^{-6} cm^2/s. The normal distance between the experimental point and the theoretical profile is calculated as a function of $\alpha'_{(0)}$, which is scanned over the same range as for the analysis of the oscillating bubble data. However, *only lower bounds on* α' can be determined from the pendant bubble profiles. (Note that this means that the adsorption kinetic constant values are also bounding values, since the ratio of adsorption to desorption kinetic constants is fixed for a given surfactant.) A typical error/point graph for the pendant bubble for the mixed-control analysis is presented in Figs. 7a and 7b; the profile asymptotes to a steady value for any α' greater than the lower bound. The mixed-control curves are shown in Fig. 8 for the pendant bubble data. The bounding values for the kinetic constants are reported in Table 4.

8. RESULTS AND DISCUSSION

The diffusion-control analysis yields an average diffusion coefficient $D'_{ave} = 7.3 \pm 0.9 \times 10^{-6}$ cm^2/s for the oscillating bubble for all data taken at frequencies less than 1 rad/s,

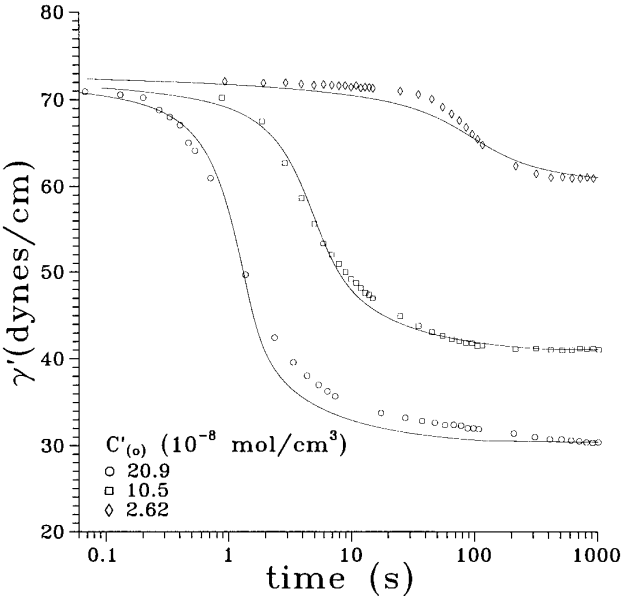

FIG. 8. The mixed-control fit of the pendant bubble relaxation experiment. The symbols represent the data. The desorption kinetic constants are reported in Table 4.

and $D'_{ave} = 6.70 \pm 0.8 \times 10^{-6}$ cm^2/s for the pendant bubble. These results are in good agreement with the pendant bubble relaxation results of Lin *et al.* (21), who report a D'_{ave} of 7×10^{-6} cm^2/s.

A mixed-control analysis of the high-concentration oscillating bubble data predicts an α' of 2.7 s^{-1} and D = 7.5×10^{-6} cm^2 s^{-1}. The mixed-control analysis applied to the lower concentrations of the oscillating bubble and to all concentrations of the pendant bubble predicted lower bounds for the desorption kinetic parameter. All of the lower bounds were less than the α' value which best fit the highest concentration data.

Amplitude Ratio: A Comparison of Theory and Experiment

The amplitude ratio $\Lambda = P_{(1)}/R_{(1)}$ of the gas-phase pressure oscillation to the radial perturbation is defined analytically in Eq. [21] of **I** as

$$\Lambda = [(4\mathrm{Ca} + 4\mathrm{Ca}_s - 2E\Gamma_{(1)_{IM}})^2 + (\Pi + 2 + 2E\Gamma_{(1)_{RE}})^2]^{1/2}. \quad [22]$$

The theoretical curves are plotted along with experimental results as a function of ω' in Fig. 9. At low ω', the curvature term dominates and Λ is approximately 2. At high ω', the deviation of the surface concentration from its equilibrium value becomes significant, and the amplitude ratio increases monotonically.

TABLE 4
Adsorption and Desorption Constants for a Mixed-Control Fit[a]

	Oscillating bubble			Pendant bubble			
$C'_{(o)}$	$\alpha'_{(o)}$[b]	α'	$\beta'_{(o)}$	$\alpha'_{(o)}$[c]	α'	$\beta'_{(o)}$	$R_{D/d}$
2.10	83.9 (b)	2.0 (b)	25.3	—	—	—	0.00549
2.62	112 (b)	2.4 (b)	33.8	23.7 (b)	0.51 (b)	7.16	0.00730
5.24	101 (b)	1.8 (b)	30.4	—	—	—	0.0199
10.5	—	—	—	16.2 (b)	0.26 (b)	4.89	0.0797
20.9	172 (m)	2.7 (m)	52.0	27.1 (b)	0.42 (b)	8.18	0.300

[a] α', 1/s; β', $\times 10^{-7}$ cm^3/mol s; $C'_{(o)}$, $\times 10^8$ mol/cm^3.
[b] Bounding values for $\alpha'_{(o)}$ at $C'_{(o)} < 2.09 \times 10^{-7}$ were found with D' fixed at 8.4×10^{-6} cm^2/s for the oscillating bubble results. For $C'_{(o)} = 2.09 \times 10^{-7}$ mol/cm^3, a two-parameter fit was performed for α' and D'.
[c] Bounding values for $\alpha'_{(o)}$ for all pendant bubble experiments were found with D fixed at 7.7×10^{-6} cm^2/s.

The amplitude ratio is determined for each experiment. In Fig. 10, the amplitude ratio for the highest concentration (2.09×10^{-7} mol cm^{-3}) is shown. The dashed curve represents the predicted profile from the diffusion-control theory. While this curve agrees well with the low-frequency results, it falls below the amplitude ratio for $\omega > 1$ rad/s. The theoretical profile for a mixed control curve for the α' and D' found from the phase angle data is the solid curve in this figure. The agreement between theory and experiment is very good. Thus, the amplitude ratio data provide an independent verification of the constants obtained from the phase angle data.

Shift in Controlling Mechanism with Bulk Concentration

The oscillating bubble data illustrate the concept of shift in controlling mechanism from diffusion control at dilute concentrations to mixed kinetic–diffusion control at elevated concentrations. This shift in controlling mechanism can be understood by considering the ratio of characteristic diffusion flux to the characteristic desorption flux as a function of bulk concentration (2, 3).

The characteristic diffusion flux toward the interface J'_D is given by

$$J'_D = D' \frac{\partial C'}{\partial r'} \approx \frac{D' C'_{(0)}}{h'}, \qquad [23]$$

where h' is the adsorption depth, a measure of the depth beneath the interface that can be depleted by surfactant adsorption:

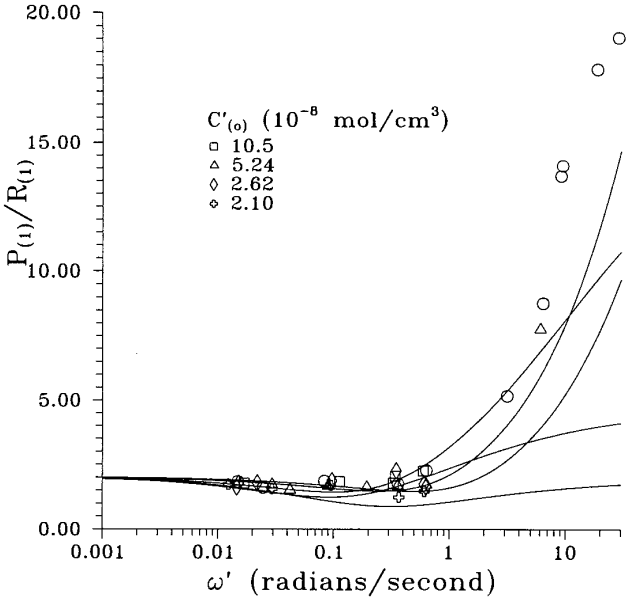

FIG. 9. The gas-phase pressure to radial amplitude ratio Λ vs ω' for the generalized Frumkin diffusion-control model.

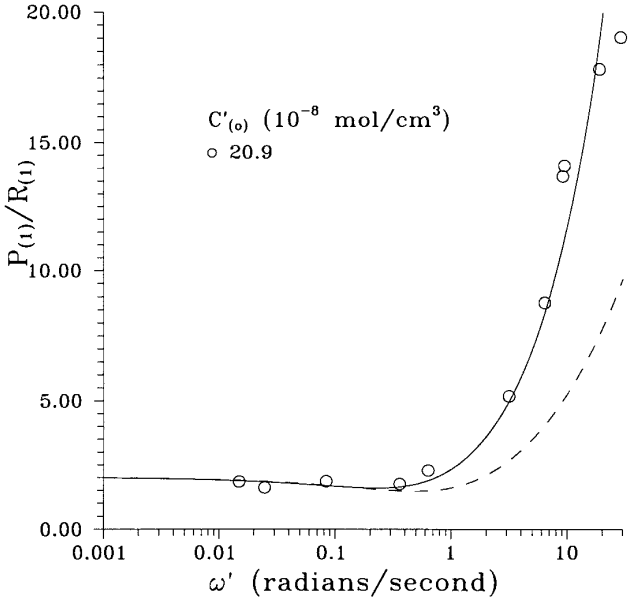

FIG. 10. The amplitude ratio Λ for $C'_{(0)} = 2.09 \times 10^{-7}$ mol/cm^3 with the mixed-control fit (solid line) and the diffusion-control result (dashed line).

$$h' = \frac{\Gamma'_{(0)}}{C'_{(0)}}. \quad [24]$$

The characteristic desorption flux J'_{des} is given by

$$J'_{\mathrm{des}} = \alpha'\Gamma' \approx \alpha'\Gamma'_{(0)}. \quad [25]$$

The ratio of the two fluxes, $R_{\mathrm{D/d}}$, becomes

$$R_{\mathrm{D/d}} = \frac{D'}{\alpha' h'^2}. \quad [26]$$

If the flux is diffusion controlled, $R_{\mathrm{D/d}}$ is small. If desorption kinetics are on the same order as the diffusion flux, $R_{\mathrm{D/d}}$ becomes order 1. Finally, if the desorption rate is smaller than the diffusion rate, $R_{\mathrm{D/d}}$ becomes large, and the system exhibits kinetic control.

Through the adsorption depth h', $R_{\mathrm{D/d}}$ depends on the bulk concentration, since h' decreases with bulk concentration. (At elevated concentrations, the ability of the interface to deplete the bulk diminishes as the interface approaches its maximum surface concentration Γ'_{∞}, and h' becomes inversely proportional to $C'_{(0)}$.)

The values for $R_{\mathrm{D/d}}$ are reported in Table 4 as a function of bulk concentration. At the lowest concentration studied, this ratio is 0.005. At the highest concentration studied, $R_{\mathrm{D/d}}$ is equal to 0.3, reflecting weak mixed kinetic–diffusion control; i.e., the desorption flux is becoming comparable to the diffusion flux. (The bulk concentration cannot be further increased in this study because 1-decanol forms a second, immiscible phase.)

The oscillating bubble was able to capture this shift in mechanism, whereas the pendant bubble was not. The greater sensitivity of the oscillating bubble method results from the ability of the forcing frequency ω' to be made comparable to the desorption kinetic time scale. If the ratio $R_{\omega} = \omega'/\alpha'$ is much less than 1, the desorption kinetics are rapid compared to the disturbance time scale, and the mixed control is not important. If R_{ω} approaches 1, the desorption rate is less than the disturbance rate, and the desorption rate must be accounted for in the behavior of the interface. Note that the mixed-control model was needed to account for the system behavior at $10 \geqslant \omega' \geqslant 1$, the range over which α' becomes comparable to ω' (i.e., $3.7 \geqslant \mathrm{R}_{\omega} \geqslant 0.37$).

Comparison with Other Studies of 1-Decanol at Aqueous–Gas Interfaces

Lin *et al.* performed a diffusion-controlled analysis of pendant bubble relaxation data of 1-decanol, finding an average diffusion coefficient of 6.5×10^{-6} cm^2/s (21), in good agreement with both our pendant bubble relaxation and our low-frequency oscillating bubble results.

Two other studies have been performed on 1-decanol adsorption in which the interface was disturbed on more rapid time scales than the pendant bubble. MacLeod and Radke (23) performed a growing drop experiment and used the Frumkin adsorption framework. In the experiment, the pressure in a growing droplet is monitored and compared to a theoretical solution for a radially growing droplet with surfactant mass transfer. The impact of gas-phase mass transfer of the volatile 1-decanol was significant in this experiment, as the droplet grows into a large gas reservoir. Data are presented for a fixed bulk concentration ($C'_{(0)} = 1.7 \times 10^{-7}$ mol/cm^3) and varying drop growth rates. The drop growth data agree well with the diffusion-controlled model, assuming small diffusion boundary layers throughout the entire drop growth process. The best fit diffusion coefficient was 8.9×10^{-6} cm^2/s for the liquid-phase transport, in reasonable agreement with results of both our oscillating and our pendant bubble studies at a similar bulk concentration ($C'_{(0)} = 1.09 \times 10^{-7}$ mol/cm^3).

Mixed kinetic–diffusion control for 1-decanol was found in a retracted pendant bubble study by Lin *et al.* (24). In this study, a pendant bubble was equilibrated in a 1-decanol aqueous solution. The bubble was then rapidly retracted, forcing the surface concentration to a value in excess of its equilibrium. The surface tension evolution is obtained by analyzing the pendant bubble shape as the surfactant desorbed in order to restore equilibrium. The authors found that a mixed-control analysis was required to explain their results, with an α' of 12.2 s^{-1} and a diffusion coefficient of 6.6×10^{-6} cm^2/s at a bulk concentration of 3.7×10^{-8} cm^2/s. At this concentration, the oscillating bubble data agreed with a diffusion-control model. However, in the retracted pendant bubble experiment, the surface concentration is significantly concentrated above its equilibrium, increasing the driving force for desorption from the retracted bubble interface significantly above that which applies at the equilibrium surface concentration.

Therefore, the results for 1-decanol adsorption kinetics in the literature either support the results obtained here by the oscillating bubble method or differ in a manner that can be explained by the different nature of the interfacial disturbances (i.e., strong (for the retracted bubble) or weak (for the oscillating bubble) disturbances from a surface equilibrium state).

9. CONCLUSIONS

In this paper, the effectiveness of the oscillating bubble method was demonstrated as a precise tool for measuring surfactant mass transfer kinetics. The phase angle between the forced radial oscillations and the gas-phase pressure os-

cillations was measured and compared to theoretical profiles based on a linear analysis of the governing equations. For the 1-decanol–aqueous system, the mass transport of 1-decanol was clearly demonstrated to obey a diffusion-controlled mass transfer model for systems that are sufficiently dilute and disturbances that are sufficiently slow (e.g., the pendant bubble relaxation method and the oscillating bubble method for $\omega' < 1$ rad/s). For faster time scale disturbances at higher frequencies, the oscillating bubble method showed the mass transport of 1-decanol to be mixed diffusion–kinetic-controlled. These data are in qualitative agreement with those obtained in a pendant bubble retraction study by Lin *et al.*, in that mixed kinetic–diffusion control is observed. However, our desorption coefficient is roughly four times smaller than that for the retracted bubble. This discrepancy may be attributed to the strong enrichment of the interface caused by the significant contraction of the retracted pendant bubble interface that significantly enriches the interface above its equilibrium and slows the desorption coefficient below that which applies at the equilibrium surface concentration. Finally, the kinetic parameters found from analyzing phase angle measurements agree excellently with the amplitude ratio data for the oscillating bubble (i.e., the ratio of the amplitude of the gas-phase pressure oscillation to that of the bubble radius). Thus, the amplitude ratio provides an independent verification of the kinetic constants obtained from the phase angle data.

REFERENCES

1. Johnson, D. O., and Stebe, K. J., *J. Colloid Int. Sci.* **168,** 21 (1994).
2. Lin, S. Y., *et al., J. Chem. Eng. Jpn.*, in press.
3. Pan, R., *et al., J. Colloid Interface Sci.*, in press.
4. Metcalfe, I. L., Enhorning, G., and Possmayer, F., *J. Appl. Physiol.* **49,** 34 (1980).
5. Enhorning, G., *J. Appl. Physiol.* **43,** 198 (1977).
6. Yu, S. H., and Possmayer, F., *Biochim. Biophys. Acta* **961,** 337 (1988).
7. Hall, S. B., *et al., J. Appl. Physiol.* **75,** 468 (1993).
8. Chang, C. H., and Franses, E. I., *J. Colloid Interface Sci.* **164,** 107 (1994).
9. Chang, C. H., and Franses, E. I., *Chem. Eng. Sci.* **49,** 313 (1994).
10. Park, S. Y., *et al., Langmuir* **9,** 3640 (1993).
11. Wantke, K. D., Miller, R., and Lunkenheimer, K., *Z. Phys. Chem. Leipzig* **261,** 1177 (1980).
12. Lunkenheimer, K., and Miller, R., *Z. Phys. Chem. Leipzig* **265,** 71 (1984).
13. Lunkenheimer, K., Hartenstein, C., Miller, R., and Wantke, K. D., *Colloid Surf.* **8,** 271 (1984).
14. Wantke, K. D., Lunkenheimer, K., and Hempt, C., *J. Colloid Interface Sci.* **159,** 28 (1993).
15. Lu, H. L., and Apfel, R. E., *J. Colloid Interface Sci.* **134,** 245 (1990).
16. Hsu, C. J., and Apfel, R. E., *J. Colloid Interface Sci.* **107,** 467 (1985).
17. Tian, Y., Holt, R. G., and Apfel, R. E., *Phys. Fluids* **7**(12), 2938 (1995).
18. Lucassen, J., and Hansen, R. S., *J. Colloid Interface Sci.* **22,** 32 (1966).
19. Lin, S. Y., McKeigue, K., and Maldarelli, C., *AIChE J.* **36,** 1785 (1990).
20. Rotenburg, Y., Boruvka, L., and Neumann, A. W., *J. Colloid Interface Sci.* **93,** 169 (1983).
21. Lin, S. Y., McKeigue, K., and Maldarelli, C., *Langmuir* **7,** 1055 (1991).
22. Johnson, D. O., Ph.D. Thesis, 1996.
23. MacLeod, C., and Radke, C. J., *J. Colloid Interface Sci.* **166,** 73 (1994).
24. Lin, S. Y., Lu, T. L., and Hwang, W. B., *Langmuir* **11,** 555 (1995).